Bone Quality in Zebrafish Vertebrae Improves After Alendronate Administration in a Glucocorticoid-induced Osteoporosis Model

Fabio Rocha Bohns[1,2,3], Riaz Akhtar[2], Yung-Jen Chuang[4], Po-Yu Chen[1*]

[1]Department of Materials Science and Engineering, National Tsing Hua University, Hsinchu, Taiwan

[2]Department of Mechanical, Materials and Aerospace Engineering, University of Liverpool, Liverpool, UK

[3]International Intercollegiate Ph.D. Program, National Tsing Hua University, Hsinchu, Taiwan

[4]School of Medicine, National Tsing Hua University, Hsinchu, Taiwan

Abstract

Glucocorticoid-induced osteoporosis (GIOP) changes the microarchitecture of bones and often leads to the reduction of bone-mineral density (BMD) and increased fracture rates. Zebrafish has been used as an alternative model for GIOP, however, the interaction of GIOP, and its treatment, with zebrafish bone morphometrics and mechanical properties, remains a challenge. Thus, this study aimed to evaluate the effects of prednisolone and alendronate on the properties of zebrafish vertebrae. Adult 7-month-old zebrafish were distributed into four groups: control (CTRL), prednisolone-only (PN), alendronate-only (ALN), and the sequential use of both medicines (PN + ALN). Fish skeletons were scanned via micro-tomography (n = 3) to obtain vertebra morphometrics (e.g., BMD). Bone morphology was assessed using scanning electron microscopy (n = 4) and the biomechanical behaviour with nanoindentation technique (n = 3). The BMD decreased in PN (426.08 ± 18.58 mg/cm^3) and ALN (398.23 ± 10.20 mg/cm^3) groups compared to the CTRL (490.43 ± 41.96 mg/cm^3) ($p < 0.001$); however, administering the medicines in sequence recovered the values to healthy levels (495.43 ± 22.06 mg/cm^3) ($p > 0.05$). The bone layered structures remain preserved in all groups. The vertebrae of the groups that received ALN and PN + ALN, displayed higher modulus of elasticity (27.27 ± 1.59 GPa and 25.68 ± 2.07 GPa, respectively) than the CTRL (22.74 ± 1.60 GP) ($p < 0.001$). ALN alone increased the hardness of zebrafish vertebrae to the highest value among the treatments (1.32 ± 0.13 GPa) ($p < 0.001$). Conversely, PN + ALN (1.25 ± 0.11 GPa) showed unaltered hardness from the CTRL (1.18 ± 0.13 GPa), but significantly higher than the PN group (1.08 ± 0.12 GPa) ($p < 0.001$). ALN administered after GIOP development, rescued osteoporotic condition by recovering the BMD and bone hardness in zebrafish vertebrae.

zebrafish; osteoporosis; biomechanics; bone matrix; drug effects

1. Introduction

Bone is an anisotropic heterogeneous mineralised tissue composed by hydroxyapatite (HAp) crystals and collagen fibres tightly entangled into a complex hierarchical structure (Meyers et al., 2013). Bones shape the body structure, sustain vertebrates' body weight and produce the skeletal cells responsible for the lifelong cycles of bone remodelling (i.e., osteoblasts and osteoclasts), a paramount process to vertebrates' life maintenance (Delaisse et al., 2020; Eriksen, 1986). In orderly conditions, the dynamic processes of bone resorption by osteoclasts and bone formation by osteoblasts are in a state of homeostasis (Chandra and Rajawat, 2021; Delaisse et al., 2020; Eriksen, 1986). If the bone removal rate surpasses the rate of bone formation (bone catabolism), the individual might develop mineralised tissues diseases (e.g., osteoporosis) (Chandra and Rajawat, 2021). Osteoporosis decreases the characteristic bone-mineral density (BMD) of healthy bones, modifying their microstructure, and increasing the susceptibility to fractures (Genest et al., 2021; Iba et al., 2020). The disease arises as a major concern among the bone metabolic diseases due to its prevalence, especially in post-menopausal women (primary osteoporosis) and in those people receiving long-term (> 6 months) or high-dose treatment with glucocorticoids (secondary osteoporosis) (Axelsson et al., 2017; Chandra and Rajawat, 2021; Chotiyarnwong and McCloskey, 2020; Hassler et al., 2015). In the near future, osteoporosis will require enormous healthcare resources and will cause economic burden across Europe (Yeh et al., 2023).

Prednisolone is a widely prescribed glucocorticoid for treating a wide range of conditions such as inflammation and autoimmune diseases and is attractive due to its low price (Chotiyarnwong and McCloskey, 2020; Vandewalle et al., 2018). However, its application is hampered due to side effects that includes secondary osteoporosis, namely glucocorticoid-induced osteoporosis (GIOP), among others (Vandewalle et al., 2018). GIOP is the most prevalent cause of secondary osteoporosis and requires attention in its symptoms and outcomes

(Chotiyarnwong and McCloskey, 2020). The pathophysiology of GIOP starts with an elevated rate of bone resorption by osteoclasts, followed by an inhibition in osteoblastogenesis (Chotiyarnwong and McCloskey, 2020; Vandewalle et al., 2018). People receiving treatment with prednisolone are recommended to concomitantly maintain regular physical activities and have an adequate diet; if increased risk of fractures are diagnosed, it is recommended intervention with anti-resorptive agents such as drugs from the bisphosphonates family (Chotiyarnwong and McCloskey, 2020). Alendronate is an alkyl-amino bisphosphonate with high affinity in binding to the bones and related to promote osteoclasts apoptosis, decreasing the rate of bone resorption (Russell, 2007); consequently, the compound can counteract with the outcomes of both primary (Hassler et al., 2015; Iba et al., 2020) and secondary osteoporosis (Chotiyarnwong and McCloskey, 2020). To improve our understanding about GIOP and its treatments, vertebrate *in vivo* model's alternative to mammals have been suggested (Barrett et al., 2006).

Zebrafish (*Danio rerio*) are small teleost fish with strong genetic similarities to humans and relative rapid bone maturation (Lin et al., 2022). Zebrafish are considered a powerful model to diverse diseases, including GIOP (Lin et al., 2022, 2019). The GIOP pathology exacerbation in zebrafish was first introduced by Barret and colleagues (Barrett et al., 2006). The protocol consists in mixing prednisolone into fish tank water, so that the fish absorb the compound with their operculum and through body osmosis; anti-resorptive agents can be administered in similar fashion (Pasqualetti et al., 2015). Stained bones observation under fluorescence signal is widely used for GIOP identification in zebrafish since it is a low cost and rapid technique (Barrett et al., 2006; Geurtzen et al., 2017; Lin et al., 2019) for the longitudinal follow-up of the same fish (Bohns et al., 2020; Cardeira et al., 2016). However, more robust techniques (i.e., tomography) have been proposed to investigate zebrafish's skeleton development (Bird and Mabee, 2003), genetic mutations (Charles et al., 2017) and bone defects (Lin et al., 2019), and

has potential for application in GIOP diagnosis and medicine effects in zebrafish. The availability of zebrafish for bone-related diseases evaluation, makes them suitable substitutes to rodents, contributing to the 3 Rs (Replacement, Reduction and Refinement) in ethical Guidelines for animal research (Embry et al., 2010).

Despite the advances in our understanding of GIOP model and its treatments, we still lack information on the bone's mechanical and morphometric qualities (Axelsson et al., 2017; Bohns et al., 2020). Hence, this study aimed to further clarify the interaction between anti- and pro-mineralogenic compounds, administered alone or in sequence, and the quality of vertebral bone in zebrafish model. We approached the subject by assessing the BMD, and other morphometric parameters, with micro-computed tomography (μ-CT), as well as the biomechanical values (with nanoindentation) of zebrafish vertebrae after the onset of GIOP and the treatment with bisphosphonate.

2. Material and Methods

2.1. Materials and reagents

Prednisolone, Tricaine (MS-222), Sodium Chloride (NaCl; MW: 58.440 g/mol) and Potassium Phosphate (KH_2PO_4; MW: 136.086 g/mol) were purchased within Sigma Aldrich, Missouri, MO, US. Alendronate and Isoflurane were obtained from Alfa Aesar, Loughborough, Leicestershire, UK. Dimethyl sulfoxide (DMSO), Sodium Hypochlorite (NaClO; 5% solution), Sodium Phosphate (Na_2HPO_4; MW: 141.960 g/mol) and Potassium Chloride (KCl; MW: 74.550 g/mol) were obtained from J.T. Baker, Pennsylvania, PA, USA. The cryomolds and Optimal Cutting Temperature compound (OCT) were obtained within TissueTek®, Sakura Finetek Europe B.V., Netherlands. Regular viscosity epoxy resin (EpoFix Kit 550 mPa.s) was obtained within Struers Inc., Cleveland, OH, US.

2.2. Zebrafish information and experimental approval

Twenty-six (n = 26) seven-month-old wild-type AB strain zebrafish of both sexes, measuring 26.09 ± 2.16 mm in length, were obtained from the Taiwan Zebrafish Core Facility at Academia Sinica (TZCAS). In accordance with the United Nations (World Population Prospects 2022), the life expectancy, for combined genders, in the World is ~72 years old; the fish used in this research would then be comparable to human adolescents with 14 years old, representing 19.4% of human average lifespan.

Until the experimentation, the fish were maintained in an environment with recirculating water system, with daily light/dark (l/d) cycles at 28°C, and fed twice a day (Westerfield, 2000). The experimental use of zebrafish was backed by the Experimental Animal Care and Use Committee of NTHU (IACUC approval number: 10048). This research was conducted in accordance with the Animal Research: Reporting of *in vivo* Experiments (ARRIVE) guidelines (Percie du Sert et al., 2020). The *n* used in each experiment was decided based on previous pilot studies and anticipating loss of individuals during medication management (Bohns et al., 2020). No animals were excluded from the research. The experiments were not blinded.

2.3. Experimental groups allocation

The fish were randomly assigned to numbered containers with 120 mL of water. Each fish was kept in a separated tank throughout the experimentation. The containers were then randomly allocated into four groups depending on the treatment proposed using the function "*rand()*" in Microsoft Excel.

Two different concentrated stock solutions containing Prednisolone or Alendronate were prepared and stored under refrigeration during the experimentation: The stock solution (A) had Prednisolone dissolved in DMSO, while the stock solution (B) had Alendronate dissolved in tank water.

In seven of the tanks (n = 7), the stock solution A was diluted in the fish tank water to a final concentration of 50 µM (Geurtzen and Knopf, 2018). The fish remained inside the tanks for 21 days and 1/3 of the water with the relative proportion of medicine was changed daily; the individuals that received this treatment were labelled as "PN". A second group composed of seven fish (n = 7) received the stock solution B diluted into the fish tank water to a final concentration of 30 µM each, for 21 days. 1/3 of water with the relative proportion of medicine was switched daily and the individuals were labelled as "ALN". In a third group of seven fish (n = 7), firstly, the fish received the stock solution A diluted to 50 µM for 21 days (Geurtzen and Knopf, 2018) and, sequentially, received the solution B diluted to 30 µM for another 21 days (42 days, in total, under treatment). For the total duration of the drugs administration, 1/3 of the water with the respective medicine was changed daily; with this it was ensured similar environment pH (Zahangir et al., 2015) and medicine concentrations at all times during experimentation. The individuals that received these interventions were labelled as "PN + ALN." The remaining five fish (n = 5) were raised for 21 days in fish tank water only and had their water changed in the same conditions as the other groups; this group was labelled as "CTRL". During the whole experimentation, the diet and l/d cycles remained unchanged. The fish were then euthanized by an overdose of Tricaine and isoflurane cocktail (Huang et al., 2010). They were properly labelled and kept at -21 °C until further use. Seven (n = 7) fish died naturally during the administration of the medicine: two (n = 2) from the PN group, three from ALN (n = 3) and two (n = 2) from PN + ALN. A flow-chart describing the experimental setup is shown in Fig. 1.

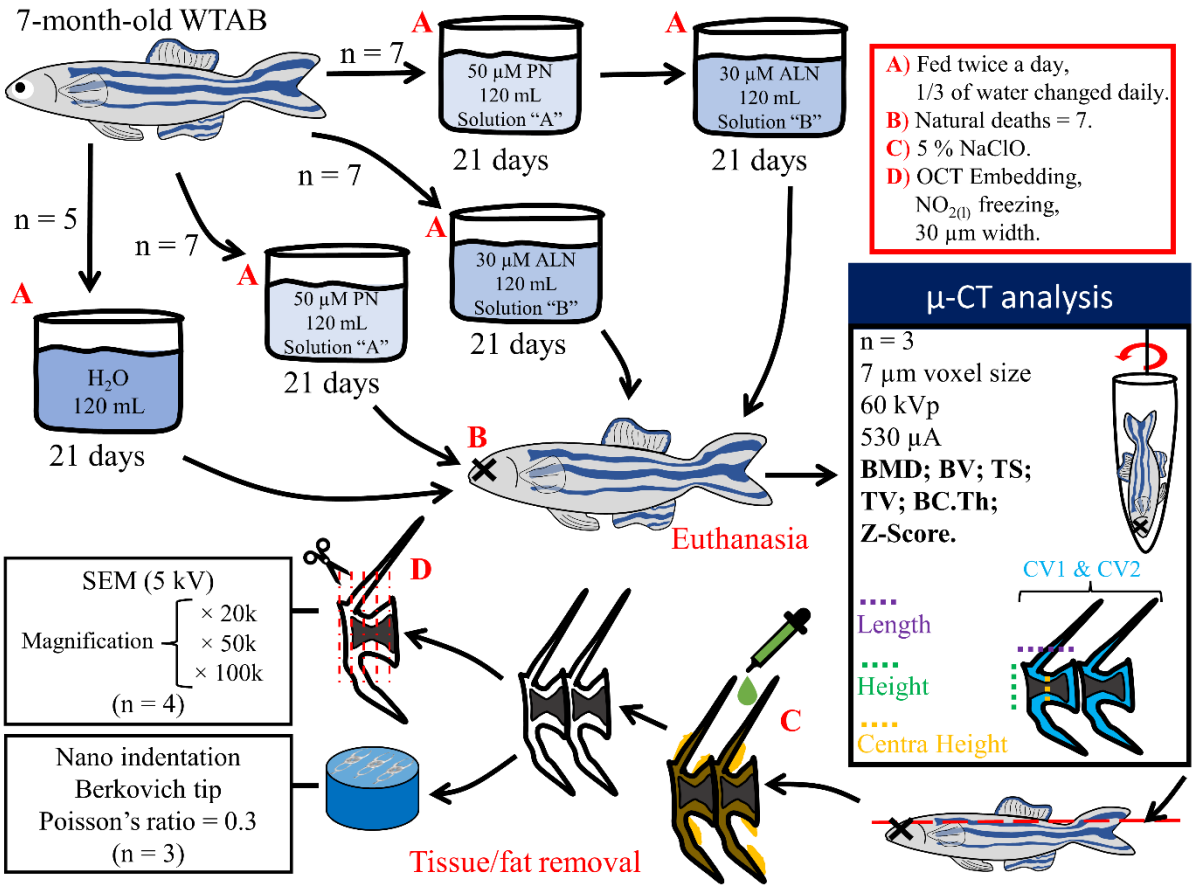

Figure 1: Flowchart containing the steps performed in this study. Fish were first treated with the corresponding medication, euthanised and scanned with µ-CT prior their vertebrae was removed for further morphological and biomechanical assessment. *(2-column fitting size - colourised).*

Three euthanized fish of each group (n = 3) were put into 11 mm diameter sample tubes and immobilized with wrapping tissue. The samples were scanned with a SkyScan 2211 Multiscale X-Ray Nanotomograph (Bruker; Massachusetts, MA, US) in air. After analysis, each fish was put into the freezer at -21 °C until they were further used. The detailed images were obtained with a voxel size of 7 µm with micro-focus scanning. The equipment voltage was set to 60 kVp, the current used was 530 µA, with 6-Watt output. The image reconstruction was performed and corrected by reconstruction software (Instarecon; Illinois, IL, US). Reconstructed cross-sections were reoriented, and the Region of Interest (ROI) was chosen. Scans of the vertebral

columns were performed at 700 µm diameter / 100 pixels, and the bone volume (BV), tissue volume (TV) (Monma et al., 2019), and cortical bone thickness (B.Th) (Hildebrand and Rüegsegger, 1997) for both caudal vertebrae 1 and 2 (CV1 and CV2, respectively) were calculated. Similarly, the BV / TV was deduced based in the data obtained. The BMD of CV1 and CV2 were also assessed using a software supplied by the instrument manufacturer (CTAn v.1.18; Bruker, Illinois, IL, US). BMD measurements were calibrated using phantoms of known HAp density. Z-Scores were calculated based on the BMD values of CTRL zebrafish (Genest et al., 2021). For further morphometric analyses, we have used CTVox (Bruker, Illinois, IL, US) and DataViewer (Bruker, Illinois, IL, US) software, also supplemented by the manufacturer. Further morphometric analyses of the ROI were performed using ImageJ 1.52a (Wayne Rasband, National Institutes of Health, Bethesda, MD).

2.4. Vertebra segments separation

Zebrafish were positioned individually onto microscope glass slides, and, with a scalpel, an incision was performed below the first dorsal stripe. Using n° 5 tweezers, the cavity was maintained opened, and the tissues adjacent to the backbone were carefully removed. Gently, the fish had their vertebral column extracted and put onto a petri dish; the excess of tissue was removed with 5% NaClO solution, and by further mechanical removal with a scalpel. The vertebra segments belonging to the pre-caudal (PC1 to PC10) and caudal vertebra (CV1 to CV14) were disconnected from each other, numbered relative to their position, and stored at -21 °C in 24-well plates. The vertebrae segments from the Weberian apparatus and the endpoint of the caudal fin were not used in this research but were stored for training purposes.

2.5. Mineralised tissue morphology

PC vertebra segments of different zebrafish (n = 4) were positioned with their axial or sagittal surface facing the bottom of cryomolds. The cryomolds were filled with OCT and indirectly frozen with liquid nitrogen until they became opaque-white. The then solid moulds

were wrapped in aluminium foil and stored at -21 °C until use. The OCT blocks were cut into slices of 30 µm of thickness with a microtome CM3050 S (Leica Microsystems GmbH; Wetzlar, Germany), and the generated axial and sagittal pieces were fixed onto microscope glass slides. The slides were further cleaned from the excess of OCT with phosphate-buffered solution (PBS), formulated with NaCl, KH_2PO_4, Na_2HPO_4 and KCl (Chazotte, 2012), with its pH adjusted to ~7.4. Then, the slices were dried and were transferred to aluminium stubs properly covered with conductive copper tape; the samples had their surface sputtered with a thin layer of platinum for 90 seconds and the bone morphologies were observed with a Scanning Electron Microscope SU8010 (SEM; Hitachi, Chiyoda, Japan) at 5 kV.

2.6. Nanoindentation

CV bones were positioned and fixed in the bottom of plastic metallography moulds with their axial surface facing down. The moulds were poured gently with epoxy resin, let to set overnight and were ground with silicon-carbide (SiC) papers and polished with 0.2 µm alumina slurry. A nanoindenter G200 system with a DCM-II head (KLA-Tencor, California, CA, US) and equipped with a Berkovich (three-sided pyramidal) tip with 20 nm radius was used. The elastic modulus (*E*) and hardness (*H*) of the samples were calculated via Oliver and Pharr method (Oliver and Pharr, 2004, 1992). A Poisson's ratio of 0.3 was assumed for the bone samples. Bones of three different zebrafish (n = 3) per group were measured. The indentations had their load controlled to 0.5 µN and the holding times were set to 0 s each. All the biomechanical testing was conducted in temperature-controlled laboratory at 22 °C. Multiple indentations were conducted distant to each other to alleviate interaction effects between two measurements.

2.7. Statistical analysis

The data was assessed for normality using Shapiro-Wilk test. Parametric or non-parametric statistical methods were chosen depending on if results passed or failed the normality test. The numerical values obtained with µ-CT passed the normal distribution test ($p > 0.01$) and were analysed with One-Way ANOVA followed by Dunn's post-hoc test for comparisons against the control ($p < 0.01$); the nano-hardness and elastic modulus passed normality test ($p < 0.01$) and were thus analysed with One-Way ANOVA and Dunn's post-hoc test for pairwise comparisons ($p < 0.01$). All statistical analysis was conducted with Sigma Plot 14.5 (Systat Software; San Jose, CA). In addition, descriptive analyses were performed on skeleton features obtained with µ-CT scans and in the morphology of mineralised tissue visualised with SEM.

3. Results

3.1. Bone morphometry and mineral density

Three fish of each group were randomly selected and scanned with µ-CT. Their skeletal characteristics are shown in Fig. 2. When set to the same pixel range, PN and ALN had lower intensity signals if compared to CTRL (Fig. 2a). Lower signals obtained with µ-CT are related to GIOP. On the contrary, we observed higher pixel intensities within the vertebrae of PN + ALN group. Each of the fish had the length, height and centra height of their backbone segments measured; the results are displayed in the Supplemental Fig 1. The length of CV1 and CV2 vertebrae were normalized with their respective radius (height/2); this minimized the effects of comparing different individuals. The results were plotted in the Fig. 2b. Significant decreased length/radius ratio was found in PN + ALN group in comparison to the CTRL ($p < 0.05$), which demonstrates an alteration in the proportion of the vertebrae.

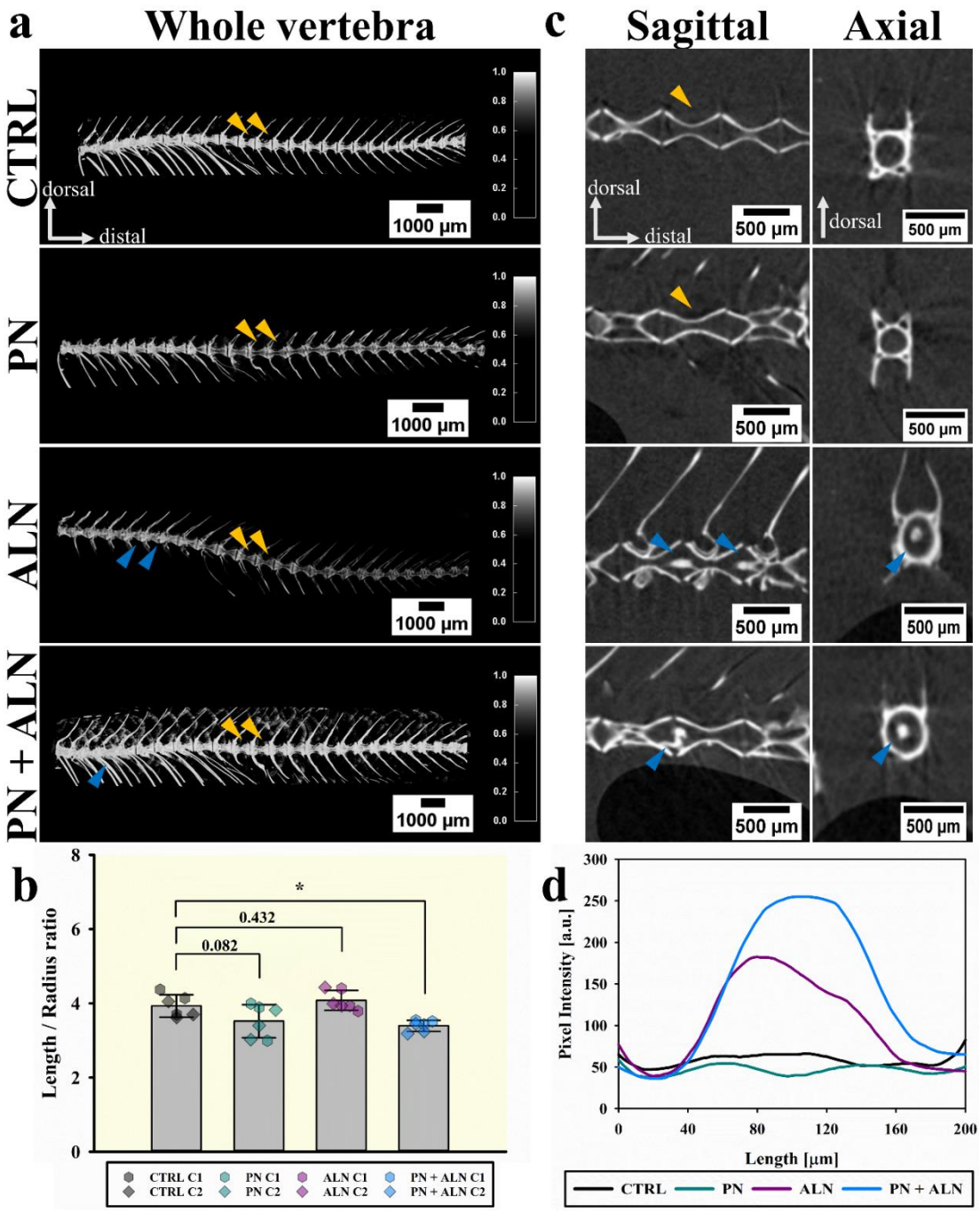

Figure 2: Montage with the various features of the zebrafish skeleton obtained with µ-CT scan. (a) Isolated whole vertebrae of CTRL, PN, ALN and PN + ALN representative samples; (b) Ratio between the length and radius; (c) Sagittal and axial views showing lumps of mineralisation in the centra of ALN and PN + ALN groups; (d) pixel intensity measured from side-to-side of the axial surface of single vertebra. High pixel intensities show the mineralised lumps signals found in ALN and PN + ALN groups. The blue arrowheads show the position in

which the abnormal minerals were found. The yellow arrowheads show the CV1 and CV2 vertebrae; they were used for the purposes of calculations in this research. Significance: * < 0.05, ** < 0.01 and **** < 0.001. *(2-column fitting size - colourised).*

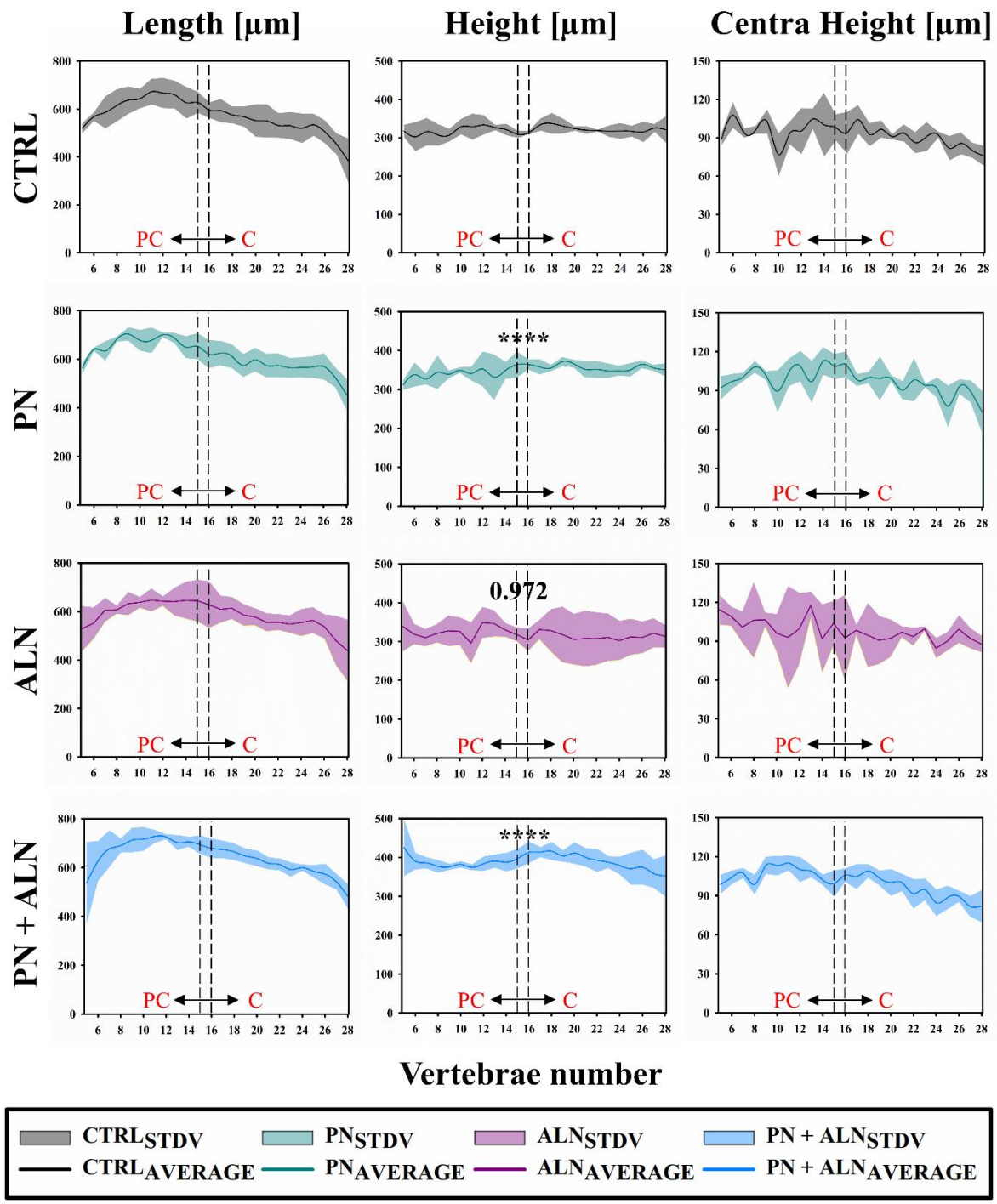

Supplemental Figure 1: Measured length, height and centra height of zebrafish. Significance: * < 0.05, ** < 0.01 and **** < 0.001. *(2-column fitting size - colourised).*

Bone details inside the vertebral cavity can be seen with sagittal and axial cuts (Fig. 2c). Mineralisation sites were found within the vertebra segments of ALN and PN + ALN fish; CTRL and PN groups did not displayed any sign of similar ossification. The calcifications were found connecting two different vertebrae bones (e.g., PC5 to PC6 and PC6 to PC7 in ALN group) and had either a hollow or a filled core. Moreover, they have at least one point of connection to the vertebral body. The internal ossifications found in PN + ALN group had higher pixel intensity than ALN alone (Fig. 2d).

The various volumetric and surface measurements performed with the reconstruction software are displayed in the Fig. 3a-c. We have first assessed the BV characteristics; PN + ALN group have shown significantly higher values in comparison to CTRL ($p < 0.001$); conversely, TV values showed a low range variation from $2.77 \times 10^{-6} \pm 8.59 \times 10^{-7}$ cm^3 (ALN) to $3.11 \times 10^{-6} \pm 7.48 \times 10^{-7}$ cm^3 (PN + ALN), with no significant effect of the medicines ($p > 0.05$). The B.Th of PN and PN + ALN groups showed increased values than CTRL group ($p < 0.05$ and $p < 0.01$, in this order). Next, we divided the BV by the TV (Fig. 3d). The parameter defined by the bone volume relative to the tissue volume (BV / TV) is an important parameter for bone diseases diagnosis, however, has shown no significant difference among the groups ($p > 0.05$). BMD measurements are shown in the Fig. 3e. Differently from BV / TV, the BMD of PN and ALN displayed lower values than CTRL ($p < 0.001$); this not simply reaffirm the potential of PN in decreasing the BMD in zebrafish vertebrae, but also showed that ALN, if administered alone, may decrease the BMD. PN + ALN displayed similar range of BMD values to CTRL ($p > 0.05$). The Z-Scores are represented in the Fig. 3f; corroborating with mineral density results, the Z-Scores of both groups (PN and ALN) were found on the bottom part of

the graph, within the range of osteopenia/osteoporosis (from -1 to -3), while PN + ALN values were in the range of CTRL bones (from -1 to 1).

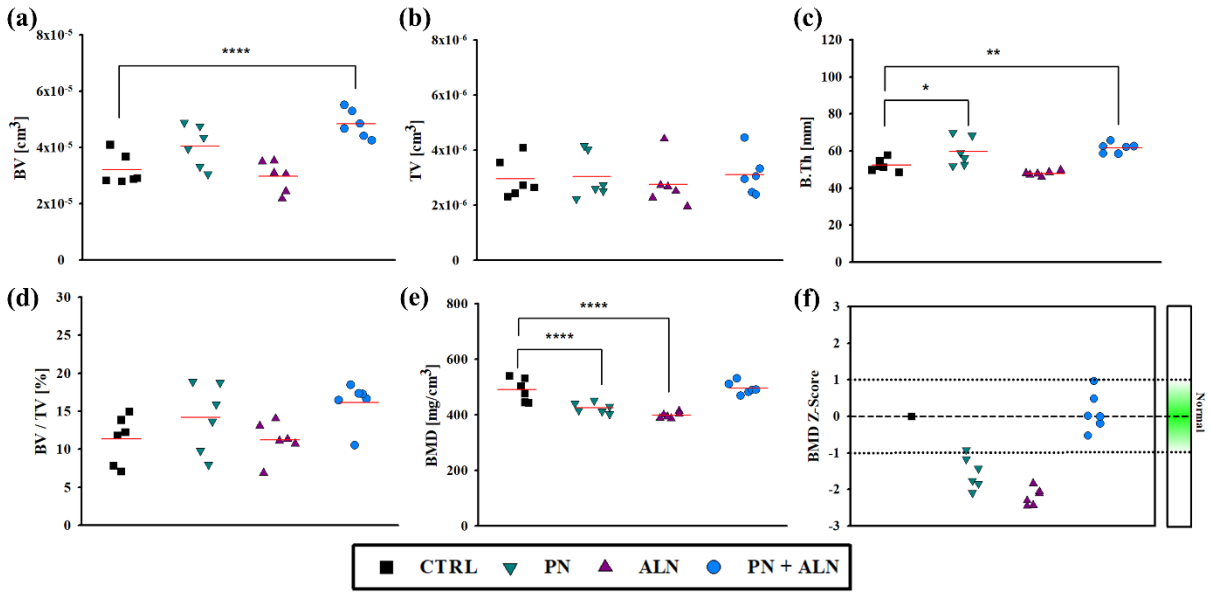

Figure 3: Morphometric data obtained with µ-CT: (a) BV; (b) TV; (c) B.Th; (d) BV / TV; (e) BMD. Z-Scores calculated based on the BMD levels of CTRL group fish. Significance: * < 0.05, ** < 0.01 and **** < 0.001. *(2-column fitting size - colourised).*

3.2. Bone morphology

The bone morphologies are displayed in the Fig. 4a-l. We have highlighted ROIs containing mineralised tissues features and magnified up to ×100k; it is possible to observe that, in general, the various treatments had no effect on the natural layered structure of bones, neither on the typical carbonated hydroxyapatite surface appearance (red arrowheads in 4c, 4f, 4i, and 4l). In the CTRL group, the densely packed, greater in size, plate-like structures (yellow arrowheads in 4b-c) are predominant. Among the other groups, these structures were replaced by small-sized, highly mixed (forming an interconnected lattice), round- and plate-like structures (blue arrowheads in 4e-f, 4h-i and 4k-l). The later structures may be correlated with the use of the different treatments and the active bone remodelling on the surface of these bones.

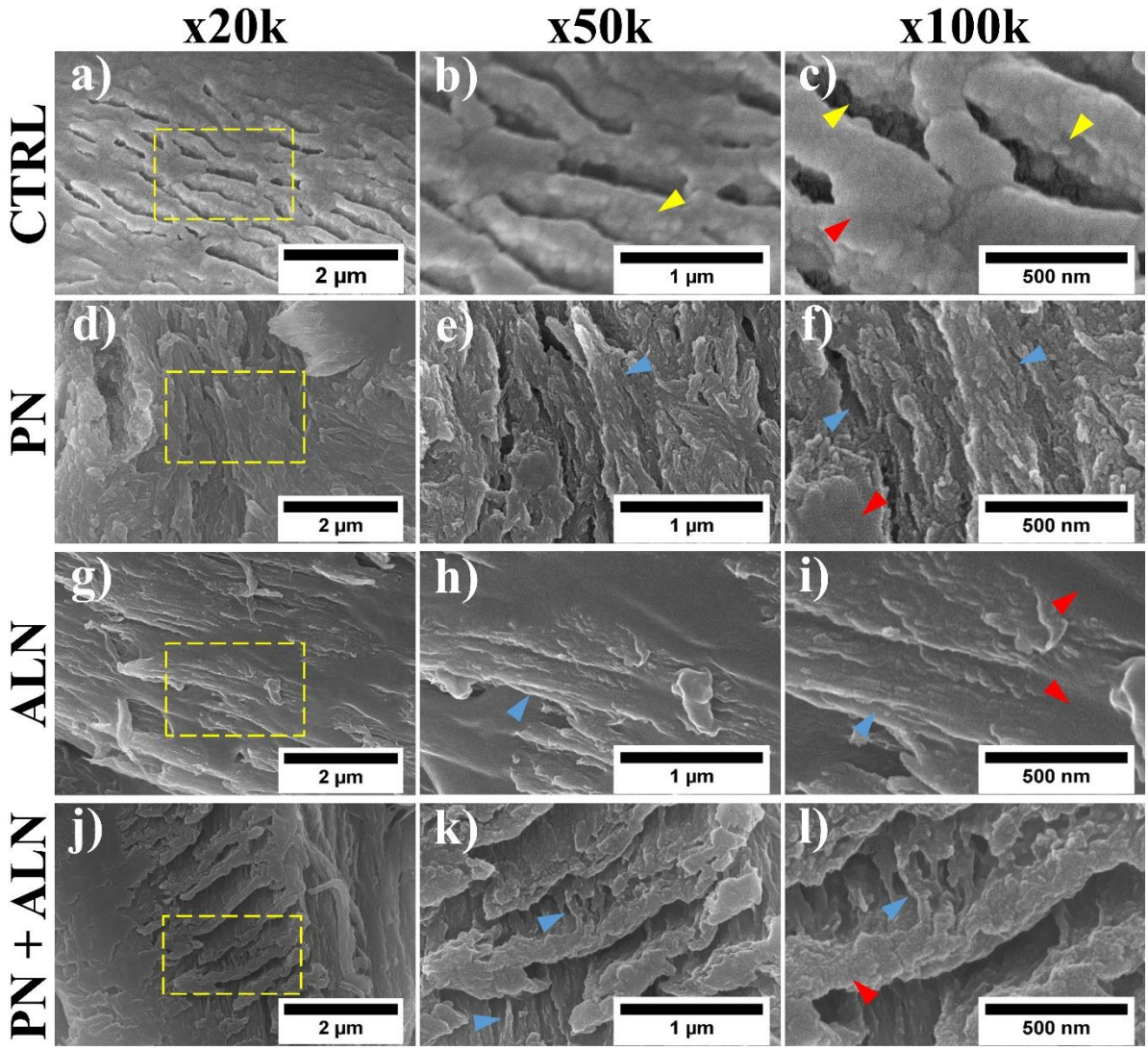

Figure 4: SEM images of 30 µm slices of zebrafish vertebrae. (4b-c) Yellow arrowheads show the deeply entangled minerals within the tissue. (4e-f, 4h-i and 4k-l) Blue arrowheads represent the small and abundant mineralised structures present in all groups that received medicine intervention. (4f, 4i and 4l) Red arrowheads highlight the carbonated HAp-like structures found in the surface of all bones, indicating the medicines do not change this natural feature. *(2-column fitting size - colourised)*.

3.3. Nano-mechanical evaluation

A series of indentations were conducted on distinct locations of the axial surface of zebrafish vertebrae (Fig. 5a). Representative load *vs*. displacement curves is shown in Fig. 5b; a lower

displacement in the bone's surfaces indicate increased mechanical properties. The plots including the results of *H* and the *E* are displayed in the Fig. 5c-d. PN group showed higher *E* heterogeneity (20.76 ± 3.46 GPa) than CTRL group (22.74 ± 1.60 GPa). However, ALN and PN + ALN reduced this heterogeneity to CTRL standard (27.27 ± 1.59 GPa and 25.68 ± 2.07 GPa, respectively). *H* of all groups displayed homogenous distribution. We found that the fish that had ALN displayed bones with higher *E* than CTRL and PN groups ($p < 0.001$). In terms of *H*, ALN alone presented the highest values overall, being significantly higher than CTRL and PN ($p < 0.001$). When ALN was used in sequence to PN (PN + ALN), the *H* increased if compared to PN ($p < 0.001$) but remained in the same range as of the CTRL fish ($p > 0.05$). Thus, ALN was able to recover the once depleted hardness of GIOP bones, to CTRL levels; this might indicate a mechanism of osteoporosis phenotype rehabilitation.

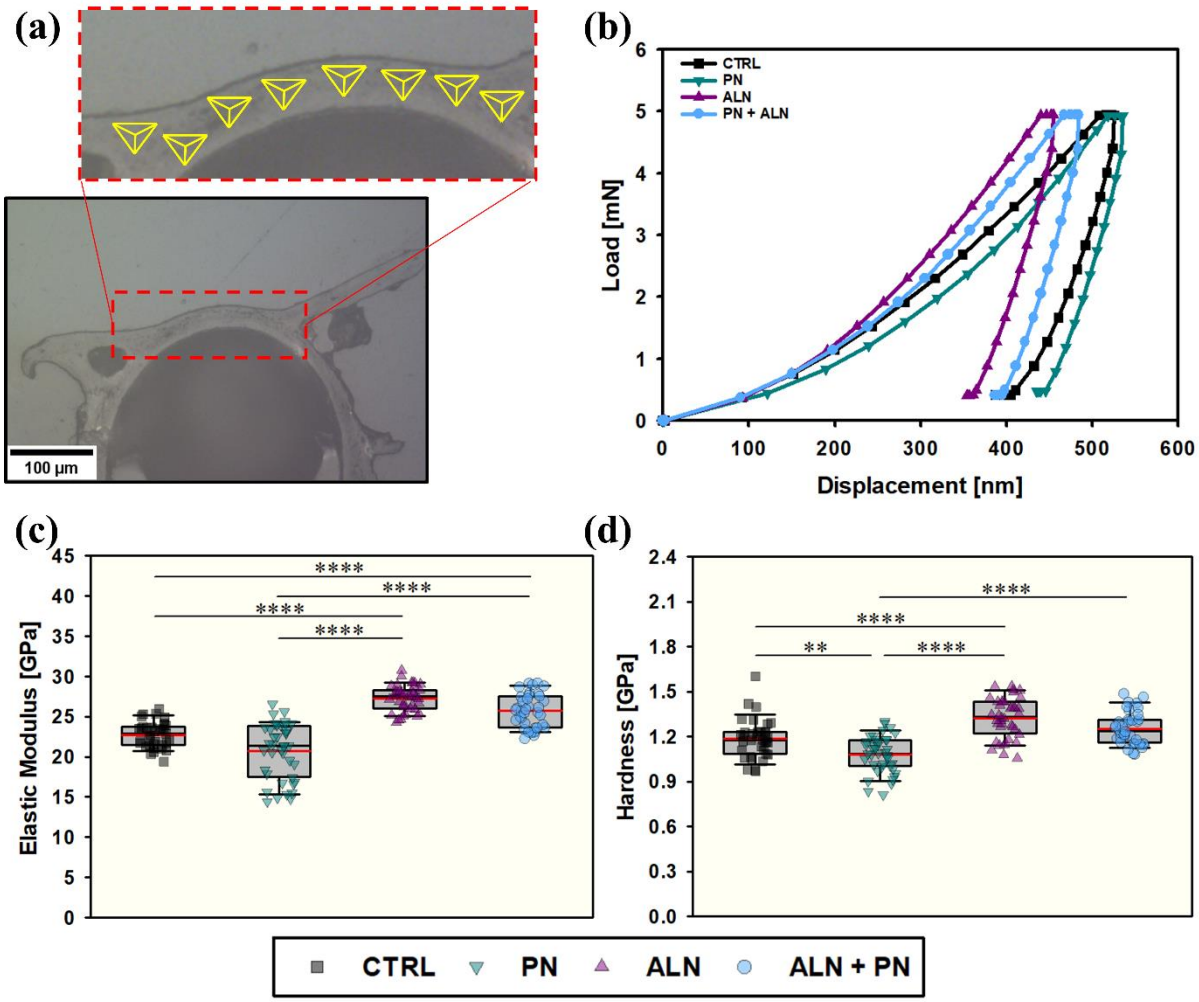

Figure 5: Scheme and results of nanoindentation (a-d). (a) Microscope view of zebrafish vertebrae axial surface, with region of interest and sketch of nanoindentation sites (as yellow pyramids). (b) Representative plot curves of nanoindentation, load vs. displacement; the load was fixed to 5 mN. (c-d) E and H results for each of the treatments proposed. Significance: * < 0.05, ** < 0.01 and **** < 0.001. *(2-column fitting size – colourised).*

4. Discussion

In this study, we explored the effects of the intake of PN and ALN, either administered alone or in succession, on the various characteristics of zebrafish vertebrae, and compare them with unmedicated fish (CTRL). Zebrafish medication was performed by adding the drugs into the fish's water. It has been reported that zebrafish consume compounds put into water by body osmosis and by their gastrointestinal tract (Pasqualetti et al., 2015); they also metabolise these

drugs similarly to other mammals (i.e., rodents and humans) (Vliegenthart et al., 2014). In a second moment, we mapped critical bone elements, such as the BMD, *E*, and *H*. We used a robust model to analyse the medicines aftermath, by the application of a well-established spatial tomography technique (Charles et al., 2017; Cotti et al., 2020; Hayes et al., 2013; Hur et al., 2017; Khajuria and Karasik, 2020; Monma et al., 2019; Silvent et al., 2017) and measured the BMD of the CV1 and CV2 of zebrafish vertebrae (Bird and Mabee, 2003; Weigele and Franz-Odendaal, 2016). Our results restate PN as a compound effective to induce GIOP, and ALN, if managed as a treatment to a previous condition, as a pro-mineralogenic agent. The affirmation of these statements occurs by the means of the reduced BMD, Z-Scores and *H* found in PN group, in opposition to the natural BMD, Z-Scores and *H* levels in PN + ALN fish (assuming natural as the values observed in the CTRL group). When ALN was consumed alone, we found lower BMD and Z-Scores, but increased mechanical properties compared to CTRL group. In addition, ALN reduced modulus' heterogeneity in zebrafish vertebrae. Our findings add to the current knowledge on bone diseases as it shows different approaches to GIOP modelled in zebrafish, with sub-tissue biomechanical analysis employed together with traditional techniques (tomography).

If fish of the same age and strain are compared, zebrafish has been demonstrated to have consistent skeleton metrics and BMD independently of their gender (Charles et al., 2017). We have used wild-type zebrafish to model GIOP due to their conserved bone physiology to humans (Barrett et al., 2006; Bruneel and Witten, 2015). The high-resolution imaging technique here applied, despite not being novel for zebrafish backbone characterisation (Charles et al., 2017; Khajuria and Karasik, 2020), demonstrated refined enough to detect small morphometric variations caused by the compounds. Similar ossifications to the ones observed inside the vertebrae cavities in ALN and PN + ALN groups, were previously reported for 45-month-old zebrafish, which also presented spine curvature (Monma et al., 2019); healthy

seven-month-old individuals are not expected to show signs of internal mineralisation, neither abnormal curved spine. Since none of the treatment regimen here used led to curved spines, we believe that bisphosphonate intake played a key role in its development. We have focused in analysing quantitatively the volumetric and bone density specifically for the CV1 and CV2 vertebrae (Bird and Mabee, 2003). Hence, the measurements performed in this study were not jeopardized by any abnormal minerals, as they were all found in the PC vertebrae. Corroborating with Geurtzen and colleagues (2017), PN showed no effect on BV of treated fish. Thus, under the settings used in our study, BV might not be an ideal parameter to identify GIOP in zebrafish.

Bone densitometry is considered a gold-standard analysis for osteopenia and osteoporosis classification (Iba et al., 2020; Khajuria and Karasik, 2020). The low values of BMD observed in the PN and ALN groups agreed with the lower signal intensities recorded using μ-CT technique. The fish that received PN were expected to present lower BMD and signal intensity values. It is widely known PN's potential to induce GIOP in zebrafish skeleton (Barrett et al., 2006; Geurtzen et al., 2017; Lin et al., 2019). The glucocorticoid mode of action in zebrafish vertebrae is still not fully clear, but it has been previously shown that, in dermal bones, it impairs osteoblast's function and decrease osteoclasts recruitment in injury sites (Geurtzen et al., 2017). Pasqualetti et al., 2015 demonstrated, using zebrafish scales, that PN treatment activates bone resorbing cells massively, recruiting them from blood circulation. The impairment of osteoblasts function, alongside with the high activation of osteoclasts in PN sites, may have significantly decreased the BMD of fish in PN group. ALN otherwise, targets resorbing osteoclasts, reducing bone removal (Russell, 2007) and stabilizing the BMD in humans diagnosed with osteoporosis (Iba et al., 2020) and in ovariectomized Wistar rats (Ma et al., 2017). We medicated healthy zebrafish solely with ALN and observed decreased BMD. Bone resorption and formation are believed to be coupled phenomena (Eriksen, 1986), and thus

ALN has been associated to decreased bone formation (Jensen et al., 2021). As consequence, in ALN only group, no therapeutic effect related to mineral density was achieved. Conversely, when ALN was administered to counteract GIOP (PN + ALN), its potential to boost previously depleted BMD, and consequently reverse the Z-Scores to healthy levels, is visible. Monma et al., (2019) compared the BMD of humans and zebrafish in terms of ageing; they demonstrated that despite BMD decreases in humans, it increases in zebrafish. Thus, BMD in zebrafish model may not behave in the same manner as expected in humans.

Since the density of diseased zebrafish bones seems to contribute more to osteoporosis determination than the bone volume alone, it is reasonable to believe the microstructures and/or the stacking of minerals was affected. We thus proposed to verify the appearance and structures of the forming minerals with imaging technique (Georgiadis et al., 2016). The zebrafish bones are composed by a different range of minerals, with different Ca/P ratios and morphologies depending on their location (Bohns et al., 2020; Mahamid et al., 2008). After treatment, it was not a surprise that the natural layered structures of bones were preserved. However, the disposal of the minerals into the mineralised collagen matrix is visually different. The minerals found in the controls, seems to be strongly entangled into the bone matrix, while the mineralised structures observed in every other group seems less entrapped within it. We assume this as the contours in CTRL group are more distinguishable and larger comparing with PN, ALN, or PN + ALN groups. The intake of medicines influenced the overall process of bone deposition and, thus, might be related to the minerals' entanglement and appearance, but not to their inherent layered hierarchical structure (Georgiadis et al., 2016; Mahamid et al., 2008). This outcome is especially important since the treatment with ALN, in an ideal situation, is not expected to affect the natural characteristics of bones (Hassler et al., 2015).

We have complemented our study by assessing the biomechanics at sub-tissue level. Nanoindentation is a powerful tool to assess small samples (Bohns et al., 2020; Zhang et al.,

2002; Zimmermann et al., 2019) and was used to evaluate the axial surface of zebrafish vertebral segments. Both *E* and *H* are important properties of bone; they both contribute to the overall mechanical strength of the tissue, being *E* strongly related to the organic content, while *H* is to the mineral phase (Ibrahim et al., 2020). The mechanical properties obtained with this method showed a decreasing trend starting from ALN > PN + ALN > CTRL > PN. The displacement generated in the bone's surfaces were around 100 nm lower in the groups with increased mechanical properties (~400 nm) at the peak force. Our measured *E* and *H*, for PN group, showed both a decrease of ~9% compared to the CTRL. Conversely, the *E* and *H* levels of ALN and ALN + PN groups increased by ~20% and ~13% their *E* and by ~12% and ~6% their *H*, respectively. A direct effect of ALN on the mechanical properties of bone is unclear (Allen, 2018). The long-term use of ALN has been related to decreased femoral head mechanics in humans (Ma et al., 2017), and significant decrease of bone *E* and contact *H* in post-menopausal women, when compared to untreated individuals (Bala et al., 2012). Another study, using nanoindentation in human cortical bone found increased hardness in bisphosphonate-treated patients in comparison to untreated (Lloyd et al., 2017). Given the discrepancy in the results, more studies involving the interaction between ALN, and bone mechanics should be carried out. In addition, the *E* data obtained from PN was more scattered than other groups, implying that GIOP increased surface heterogeneity in zebrafish vertebrae, reducing *E* values locally. It has been well documented that increased osteoclasts activity generates shallow cavities on the surface of resorbed bone (Mohamed, 2008), which affects mechanical strength. Despite the *E* in PN remained in CTRL level, the wide difference between its lowest and highest value might indicate a mechanism of bone fragility (Ibrahim et al., 2020). Yet again, with the methodology proposed, nanoindentation have shown effectiveness to distinguish small biomechanical alterations in zebrafish backbone affected by different treatment conditions.

5. Limitations

In this study, we have demonstrated, using materials science approaches, that zebrafish vertebrae have the potential to be used as a drug screening tool for bone-related diseases. However, a few limitations related to this work must be stated: (1) we did not evaluate before/after properties of the same individuals, as the euthanasia is necessary to extract the fish's vertebrae; (2) the loading environment (water) in which zebrafish lives, directly affect their remodelling ability and, consequently, bone formation (Khajuria and Karasik, 2020); (3) even though zebrafish vertebra is relatively bigger in size compared with its caudal fin bony rays, their axial surface is still very small (~50 μm) and difficult to standardize after embedded; and (4) this study did not evaluated the alterations in the properties on the sagittal direction nor in the collagen configuration. Based on previous literature, collagen arrangement within the mineralised matrix is important for bones to maintain their biomechanics. Thus, other studies should be carried to further the knowledge in bone diseases modelled in zebrafish. Additionally, studies involving cells were not the scope of this research and should be conducted in the future.

6. Conclusion

Zebrafish delivers a readily available model to study medicines interactions with mineralised tissues. Within the limitations, we have highlighted morphometric structures affected by PN and/or ALN and paralleled our findings with the biomechanical properties of zebrafish vertebrae. Despite GIOP and its treatment with ALN not showing high sensitivity with *E*, the BMD and *H* both changed with the treatments. Our approach adds to the current knowledge that ALN can rescue diseased mineralised tissues properties when administered after the onset of GIOP. This happens by the means of the restored BMD, Z-Scores and *H*.

Acknowledgements

F.R.B is funded by the University of Liverpool/National Tsing Hua University Dual Ph.D. scheme. F.R.B sincerely thank the National Science and Technology Council (NSTC), Taiwan (110-2224-E-007-003, 111-2221-E-007-084-MY3, 111-2634-F-007-008, 111-2731-M-007-001 and 111-2311-B-005-009). The authors gratefully acknowledge Dr. Haw-Kai Chang for SEM imaging. The authors sincerely thank Dr. Tzu-Hung Lin at the Industrial Technology Research Institute (ITRI) for μ-CT imaging.

7. References

Allen, M.R., 2018. Recent Advances in Understanding Bisphosphonate Effects on Bone Mechanical Properties. Curr Osteoporos Rep 16, 198–204. https://doi.org/10.1007/s11914-018-0430-3

Axelsson, K.F., Nilsson, A.G., Wedel, H., Lundh, D., Lorentzon, M., 2017. Association Between Alendronate Use and Hip Fracture Risk in Older Patients Using Oral Prednisolone. JAMA 318, 146. https://doi.org/10.1001/jama.2017.8040

Bala, Y., Depalle, B., Farlay, D., Douillard, T., Meille, S., Follet, H., Chapurlat, R., Chevalier, J., Boivin, G., 2012. Bone micromechanical properties are compromised during long-term alendronate therapy independently of mineralization. Journal of Bone and Mineral Research 27, 825–834. https://doi.org/10.1002/jbmr.1501

Barrett, R., Chappell, C., Quick, M., Fleming, A., 2006. A rapid, high content,in vivo model of glucocorticoid-induced osteoporosis. Biotechnol. J. 1, 651–655. https://doi.org/10.1002/biot.200600043

Bird, N.C., Mabee, P.M., 2003. Developmental morphology of the axial skeleton of the zebrafish,Danio rerio (Ostariophysi: Cyprinidae). Dev. Dyn. 228, 337–357. https://doi.org/10.1002/dvdy.10387

Bohns, F.R., Shih, Y., Chuang, Y., Akhtar, R., Chen, P., 2020. Influence of Prednisolone and Alendronate on the *de novo* Mineralization of Zebrafish Caudal Fin. JBMR Plus. https://doi.org/10.1002/jbm4.10435

Bruneel, B., Witten, P.E., 2015. Power and challenges of using zebrafish as a model for skeletal tissue imaging. Connect. Tissue Res. 56, 161–173. https://doi.org/10.3109/03008207.2015.1013193

Cardeira, J., Gavaia, P.J., Fernández, I., Cengiz, I.F., Moreira-Silva, J., Oliveira, J.M., Reis, R.L., Cancela, M.L., Laizé, V., 2016. Quantitative assessment of the regenerative and

mineralogenic performances of the zebrafish caudal fin. Sci. Rep. 6. https://doi.org/10.1038/srep39191

Chandra, A., Rajawat, J., 2021. Skeletal Aging and Osteoporosis: Mechanisms and Therapeutics. Int. J. Mol. Sci. 22, 3553. https://doi.org/10.3390/ijms22073553

Charles, J.F., Sury, M., Tsang, K., Urso, K., Henke, K., Huang, Y., Russell, R., Duryea, J., Harris, M.P., 2017. Utility of quantitative micro-computed tomographic analysis in zebrafish to define gene function during skeletogenesis. Bone 101, 162–171. https://doi.org/10.1016/j.bone.2017.05.001

Chazotte, B., 2012. Labeling Golgi with Fluorescent Ceramides. Cold Spring Harb. Protoc. 2012, pdb.prot070599. https://doi.org/10.1101/pdb.prot070599

Chotiyarnwong, P., McCloskey, E.V., 2020. Pathogenesis of glucocorticoid-induced osteoporosis and options for treatment. Nat. Rev. Endocrinol. 16, 437–447. https://doi.org/10.1038/s41574-020-0341-0

Cotti, S., Huysseune, A., Koppe, W., Rücklin, M., Marone, F., Wölfel, E.M., Fiedler, I.A.K., Busse, B., Forlino, A., Witten, P.E., 2020. More Bone with Less Minerals? The Effects of Dietary Phosphorus on the Post-Cranial Skeleton in Zebrafish. Int. J. Mol. Sci. 21, 5429. https://doi.org/10.3390/ijms21155429

Delaisse, J.-M., Andersen, T.L., Kristensen, H.B., Jensen, P.R., Andreasen, C.M., Søe, K., 2020. Re-thinking the bone remodeling cycle mechanism and the origin of bone loss. Bone 141, 115628. https://doi.org/10.1016/j.bone.2020.115628

Embry, M.R., Belanger, S.E., Braunbeck, T.A., Galay-Burgos, M., Halder, M., Hinton, D.E., Léonard, M.A., Lillicrap, A., Norberg-King, T., Whale, G., 2010. The fish embryo toxicity test as an animal alternative method in hazard and risk assessment and scientific research. Aquat. Toxicol. 97, 79–87. https://doi.org/10.1016/j.aquatox.2009.12.008

Eriksen, E.F., 1986. Normal and Pathological Remodeling of Human Trabecular Bone: Three-Dimensional Reconstruction of the Remodeling Sequence in Normals and in Metabolic Bone Disease*. Endocr. Rev. 7, 379–408. https://doi.org/10.1210/edrv-7-4-379

Genest, F., Claußen, L., Rak, D., Seefried, L., 2021. Bone mineral density and fracture risk in adult patients with hypophosphatasia. Osteoporos. Int. 32, 377–385. https://doi.org/10.1007/s00198-020-05612-9

Georgiadis, M., Müller, R., Schneider, P., 2016. Techniques to assess bone ultrastructure organization: orientation and arrangement of mineralized collagen fibrils. J. R. Soc. Interface 13, 20160088. https://doi.org/10.1098/rsif.2016.0088

Geurtzen, K., Knopf, F., 2018. Adult Zebrafish Injury Models to Study the Effects of Prednisolone in Regenerating Bone Tissue. J. Vis. Exp. https://doi.org/10.3791/58429

Geurtzen, K., Vernet, A., Freidin, A., Rauner, M., Hofbauer, L.C., Schneider, J.E., Brand, M., Knopf, F., 2017. Immune Suppressive and Bone Inhibitory Effects of Prednisolone in Growing and Regenerating Zebrafish Tissues. J. Bone Miner. Res. 32, 2476–2488. https://doi.org/10.1002/jbmr.3231

Hassler, N., Gamsjaeger, S., Hofstetter, B., Brozek, W., Klaushofer, K., Paschalis, E.P., 2015. Effects of long-term alendronate treatment on postmenopausal osteoporosis bone material properties. Osteoporos. Int. 26, 339–352. https://doi.org/10.1007/s00198-014-2929-5

Hayes, A.J., Reynolds, S., Nowell, M.A., Meakin, L.B., Habicher, J., Ledin, J., Bashford, A., Caterson, B., Hammond, C.L., 2013. Spinal Deformity in Aged Zebrafish Is Accompanied by Degenerative Changes to Their Vertebrae that Resemble Osteoarthritis. PLoS ONE 8, e75787. https://doi.org/10.1371/journal.pone.0075787

Hildebrand, T., Rüegsegger, P., 1997. A new method for the model-independent assessment of thickness in three-dimensional images. J. Microsc. 185, 67–75. https://doi.org/10.1046/j.1365-2818.1997.1340694.x

Huang, W.-C., Hsieh, Y.-S., Chen, I.-H., Wang, C.-H., Chang, H.-W., Yang, C.-C., Ku, T.-H., Yeh, S.-R., Chuang, Y.-J., 2010. Combined Use of MS-222 (Tricaine) and Isoflurane Extends Anesthesia Time and Minimizes Cardiac Rhythm Side Effects in Adult Zebrafish. Zebrafish 7, 297–304. https://doi.org/10.1089/zeb.2010.0653

Hur, M., Gistelinck, C.A., Huber, P., Lee, J., Thompson, M.H., Monstad-Rios, A.T., Watson, C.J., McMenamin, S.K., Willaert, A., Parichy, D.M., Coucke, P., Kwon, R.Y., 2017. MicroCT-based phenomics in the zebrafish skeleton reveals virtues of deep phenotyping in a distributed organ system. eLife 6, e26014. https://doi.org/10.7554/eLife.26014

Iba, K., Takada, J., Sonoda, T., Yamashita, T., 2020. Effect of continuous long-term treatment for 10 years with bisphosphonate on Japanese osteoporosis patients. J. Bone Miner. Metab. 38, 240–247. https://doi.org/10.1007/s00774-019-01049-1

Ibrahim, A., Magliulo, N., Groben, J., Padilla, A., Akbik, F., Abdel Hamid, Z., 2020. Hardness, an Important Indicator of Bone Quality, and the Role of Collagen in Bone Hardness. J. Funct. Biomater. 11, 85. https://doi.org/10.3390/jfb11040085

Jensen, P.R., Andersen, T.L., Chavassieux, P., Roux, J.-P., Delaisse, J.-M., 2021. Bisphosphonates impair the onset of bone formation at remodeling sites. Bone 145, 115850. https://doi.org/10.1016/j.bone.2021.115850

Khajuria, D.K., Karasik, D., 2020. Novel model of restricted mobility induced osteopenia in zebrafish. J. Fish Biol. jfb.14369. https://doi.org/10.1111/jfb.14369

Lin, W.-Y., Dharini, K., Peng, C.-H., Lin, C.-Y., Yeh, K.-T., Lee, W.-C., Lin, M.-D., 2022. Zebrafish models for glucocorticoid-induced osteoporosis. Tzu Chi Med. J. 34, 373. https://doi.org/10.4103/tcmj.tcmj_80_22

Lin, Y., Xiang, X., Chen, T., Gao, C., Fu, H., Wang, L., Deng, L., Zeng, L., Zhang, J., 2019. In vivo monitoring and high-resolution characterizing of the prednisolone-induced osteoporotic process on adult zebrafish by optical coherence tomography. Biomed. Opt. Express 10, 1184. https://doi.org/10.1364/BOE.10.001184

Lloyd, A.A., Gludovatz, B., Riedel, C., Luengo, E.A., Saiyed, R., Marty, E., Lorich, D.G., Lane, J.M., Ritchie, R.O., Busse, B., Donnelly, E., 2017. Atypical fracture with long-term bisphosphonate therapy is associated with altered cortical composition and reduced fracture resistance. Proc. Natl. Acad. Sci. U.S.A. 114, 8722–8727. https://doi.org/10.1073/pnas.1704460114

Ma, S., Goh, E.L., Jin, A., Bhattacharya, R., Boughton, O.R., Patel, B., Karunaratne, A., Vo, N.T., Atwood, R., Cobb, J.P., Hansen, U., Abel, R.L., 2017. Long-term effects of bisphosphonate therapy: perforations, microcracks and mechanical properties. Sci Rep 7, 43399. https://doi.org/10.1038/srep43399

Ma, X., Xu, Z., Ding, S., Yi, G., Wang, Q., 2017. Alendronate promotes osteoblast differentiation and bone formation in ovariectomy-induced osteoporosis through interferon-β/signal transducer and activator of transcription 1 pathway. Exp. Ther. Med. https://doi.org/10.3892/etm.2017.5381

Mahamid, J., Sharir, A., Addadi, L., Weiner, S., 2008. Amorphous calcium phosphate is a major component of the forming fin bones of zebrafish: Indications for an amorphous precursor phase. Proc. Natl. Acad. Sci. 105, 12748–12753. https://doi.org/10.1073/pnas.0803354105

Meyers, M.A., McKittrick, J., Chen, P.-Y., 2013. Structural Biological Materials: Critical Mechanics-Materials Connections. Science 339, 773–779. https://doi.org/10.1126/science.1220854

Mohamed, A.M., 2008. An overview of bone cells and their regulating factors of differentiation. Malays. J. Med. Sci. MJMS 15, 4–12.

Monma, Y., Shimada, Y., Nakayama, H., Zang, L., Nishimura, N., Tanaka, T., 2019. Aging-associated microstructural deterioration of vertebra in zebrafish. Bone Rep. 11, 100215. https://doi.org/10.1016/j.bonr.2019.100215

Oliver, W.C., Pharr, G.M., 2004. Measurement of hardness and elastic modulus by instrumented indentation: Advances in understanding and refinements to methodology. J. Mater. Res. 19, 3–20. https://doi.org/10.1557/jmr.2004.19.1.3

Oliver, W.C., Pharr, G.M., 1992. An improved technique for determining hardness and elastic modulus using load and displacement sensing indentation experiments. J. Mater. Res. 7, 1564–1583. https://doi.org/10.1557/JMR.1992.1564

Pasqualetti, S., Congiu, T., Banfi, G., Mariotti, M., 2015. Alendronate rescued osteoporotic phenotype in a model of glucocorticoid-induced osteoporosis in adult zebrafish scale. Int. J. Exp. Pathol. 96, 11–20. https://doi.org/10.1111/iep.12106

Percie du Sert, N., Ahluwalia, A., Alam, S., Avey, M.T., Baker, M., Browne, W.J., Clark, A., Cuthill, I.C., Dirnagl, U., Emerson, M., Garner, P., Holgate, S.T., Howells, D.W., Hurst, V., Karp, N.A., Lazic, S.E., Lidster, K., MacCallum, C.J., Macleod, M., Pearl, E.J., Petersen, O.H., Rawle, F., Reynolds, P., Rooney, K., Sena, E.S., Silberberg, S.D., Steckler, T., Würbel, H., 2020. Reporting animal research: Explanation and elaboration for the ARRIVE guidelines 2.0. PLOS Biol. 18, e3000411. https://doi.org/10.1371/journal.pbio.3000411

Russell, R.G.G., 2007. Bisphosphonates: Mode of Action and Pharmacology. Pediatrics 119, S150–S162. https://doi.org/10.1542/peds.2006-2023H

Silvent, J., Akiva, A., Brumfeld, V., Reznikov, N., Rechav, K., Yaniv, K., Addadi, L., Weiner, S., 2017. Zebrafish skeleton development: High resolution micro-CT and FIB-SEM block surface serial imaging for phenotype identification. PLOS ONE 12, e0177731. https://doi.org/10.1371/journal.pone.0177731

United Nations Department of Economic and Social Affairs, Population Division., 2022. World Population Prospects 2022: Summary of Results. UN DESA/POP/2022/TR/NO. 3.

Vandewalle, J., Luypaert, A., De Bosscher, K., Libert, C., 2018. Therapeutic Mechanisms of Glucocorticoids. Trends Endocrinol. Metab. 29, 42–54. https://doi.org/10.1016/j.tem.2017.10.010

Vliegenthart, A.D.B., Tucker, C.S., Del Pozo, J., Dear, J.W., 2014. Zebrafish as model organisms for studying drug-induced liver injury: Zebrafish and drug-induced liver injury. Br. J. Clin. Pharmacol. 78, 1217–1227. https://doi.org/10.1111/bcp.12408

Weigele, J., Franz-Odendaal, T.A., 2016. Functional bone histology of zebrafish reveals two types of endochondral ossification, different types of osteoblast clusters and a new bone type. J. Anat. 229, 92–103. https://doi.org/10.1111/joa.12480

Westerfield, M., 2000. The Zebrafish Book: A Guide for the Laboratory Use of Zebrafish (Danio Rerio). University of Oregon Press.

Yeh, E.J., Gitlin, M., Sorio, F., McCloskey, E., 2023. Estimating the future clinical and economic benefits of improving osteoporosis diagnosis and treatment among postmenopausal women across eight European countries. Arch. Osteoporos. 18, 68. https://doi.org/10.1007/s11657-023-01230-0

Zahangir, Md.M., Haque, F., Mostakim, G.M., Islam, M.S., 2015. Secondary stress responses of zebrafish to different pH: Evaluation in a seasonal manner. Aquaculture Reports 2, 91–96. https://doi.org/10.1016/j.aqrep.2015.08.008

Zhang, Y., Cui, F.Z., Wang, X.M., Feng, Q.L., Zhu, X.D., 2002. Mechanical properties of skeletal bone in gene-mutated stöpseldtl28d and wild-type zebrafish (Danio rerio) measured by atomic force microscopy-based nanoindentation. Bone 30, 541–546. https://doi.org/10.1016/S8756-3282(02)00676-2

Zimmermann, E.A., Riedel, C., Schmidt, F.N., Stockhausen, K.E., Chushkin, Y., Schaible, E., Gludovatz, B., Vettorazzi, E., Zontone, F., Püschel, K., Amling, M., Ritchie, R.O., Busse, B., 2019. Mechanical Competence and Bone Quality Develop During Skeletal Growth. J. Bone Miner. Res. 34, 1461–1472. https://doi.org/10.1002/jbmr.3730